CCS Chemistry

COMMUNICATION

Received: Feb. 19, 2019 | Accepted: Sept. 5, 2019

Flexible Dry Hydrogel with Lamella-Like Structure Engineered via Dehydration in Poor Solvent

Feilong Zhang[1,2], Jiajia Zhou[3], Zhen Gu[1], Man Yang[1], Siheng Li[1], Yongyang Song[1], Jun-Bing Fan[1], Jingxin Meng[1], Peiyi Wu[4], Lei Jiang[1,2,3] & Shutao Wang[1,2]*

[1]CAS Key Laboratory of Bio-Inspired Materials and Interfacial Science, CAS Center for Excellence in Nanoscience, Technical Institute of Physics and Chemistry, Chinese Academy of Sciences, Beijing 100190 (China), [2]University of Chinese Academy of Sciences, Beijing 100049 (China), [3]Key Laboratory of Bio-Inspired Smart Interfacial Science and Technology of Ministry of Education, School of Chemistry, Beihang University, Beijing 100191 (China), [4]State Key Laboratory of Molecular Engineering of Polymers, Department of Macromolecular Science and Laboratory for Advanced Materials, Fudan University, Shanghai 200433 (China)

**Corresponding author: stwang@mail.ipc.ac.cn*

Cite this: *CCS Chem.* **2019**, *1*, 533–543

Hydrogels are among the most promising biologic materials in recent technology with numerous desired applications, including serving as biosensors, drug delivery vehicles, and tissue-engineered products for cell matrices. However, they often dehydrate, and become stiff and brittle in air, causing loss of flexibility and functions. Several layered structures have been proven to increase the strength, toughness, and even flexibility of these materials, which might provide a new clue for the sustenance of the flexibility of drying gels. Herein, we report a novel solvent-dehydrated hydrogel engineering approach, aimed to change the inner structure and keep the flexibility of a dehydrated hydrogel in the air via solvent-induced dehydration, for example, acetone-dehydrated polyacrylic acid hydrogel. This flexible dry gel could be folded, twisted, and stretched without any damage due to the assumed lamella-like structures, contrary to dry gels without these microstructures or those with porous structures, which retain brittle consistency. The flexible dry gel also exhibited excellent self-healing capability with the assistance of solvents. Fascinatingly, this flexible gel film displayed strain-visualizing paper writing/erasing performance properties, with water acting as invisible ink. Thus, this fabricated flexible hydrogel film might function as confidential information storage material. Our current approach is versatile, hence applicable to other hydrogels, and provides insight into the engineering of other functional gels for extended future applications.

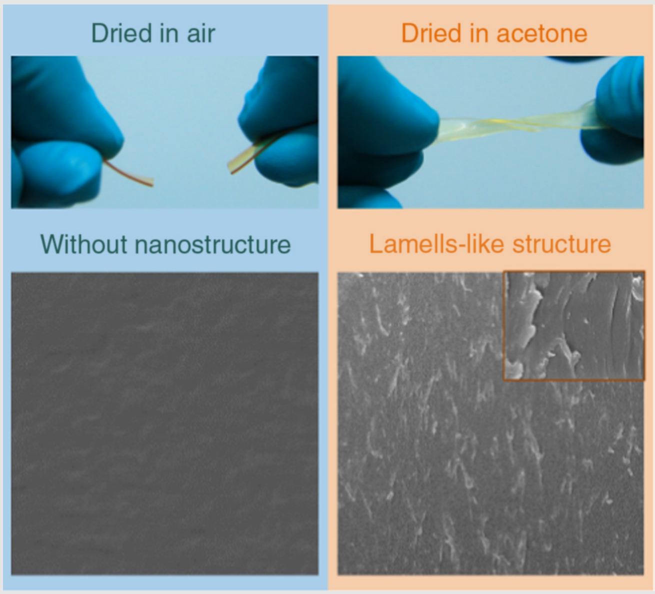

Keywords: dry hydrogel, lamella-like structure, flexible, solvent-induced dehydration, strain visualizing

DOI: 10.31635/ccschem.019.20190007

Introduction

A hydrogel is a flexible network of cross-linked hydrophilic polymer chains filled with water and has gained widespread use in diverse fields, such as biomedicine,[1–4] flexible sensors,[5,6] artificial actuator,[7,8] and others.[9–11] However, prepared hydrogels usually encounter serious problems, including losing their flexibility and becoming stiff and brittle after dehydration in air,[12,13] which hinders their development and extensive applications. For example, the modulus of polyacrylamide (PAM) hydrogel expands to ~10^8 N/m^2 from $< 10^4$ N/m^2 during air dehydration.[13] It is well-known that the physical properties of materials are not only determined by their compositions but also by their inner microstructures.[14–16] For instance, porous structures usually decrease the tensile modulus and strength of bulk materials due to crack formation around the pore when subjected to stress,[17–19] while layered structures found in nature[20–22] have proven to dissipate deformation energy without propagation of cracks, with increased strength, hardness, and toughness of these materials.[23–26] In recent years, series of artificial layered materials have been fabricated via layer-by-layer techniques,[27–29] ice-templating,[30–32] self-assembly,[21,33] and external-field-assisted assembly,[34,35] which not only exhibit increased stiffness and toughness but also high flexibility.[28] Therefore, it is an opportunity, as well as a challenge to engineer the inner microstructures of the dehydrated hydrogel in air, in favor of keeping their flexibility toward practical applications.

In a poor solvent, the hydrogels usually shrink and become opaque due to phase separation. Moreover, the phase-separated gels tend to have a bicontinuous domain structure, consisting of dense and sparse domains in the polymer network mesoscopic scale,[36–39] thereby, providing prospects for engineering the inner microstructure of dry gels, while enabling them to maintain their flexibility.

Our present report describes a strategy for engineering the inner structures of dry hydrogels in air to achieve flexibility via aqueous-phase polymerization, dehydration in a poor solvent, and drying in air to generate a solvent-dehydrated hydrogel. Compared with the non-fabricated air-dried gel, this solvent-dehydrated hydrogel maintained its flexibility and exhibited an increased toughness than that of the initial hydrogel. In addition, they were able to fold, twist, and stretch without any damage, whereas the air-dried hydrogel was hard and brittle, making it prone to breakage when bent. Moreover, in contrast to porous structured and condensed structured, brittle dry gels, our created flexible solvent-dehydrated hydrogels exhibited lamella-like structures, which might have contributed to its flexibility. Furthermore, the solvent-dehydrated hydrogels exhibited an excellent stretchable capacity, humidity-sensitivity, and solvent-assisted self-healing properties. Finally, invisible flexible/hard gel patterns could be fabricated utilizing the differences in dehydration of the hydrogel in a solvent and in air and visualized by strain sensing, which could serve as confidential information storage materials.

Results and Discussion

Engineering the inner structure of dry PAA film

We used polyacrylic acid (PAA) hydrogel as an example with acetone as the poor solvent and engineered through solvent-induced dehydration of PAA hydrogel in acetone to generate acetone-dehydrated PAA (acetone-DPAA) hydrogel. The original PAA hydrogel film was fabricated by free-radical polymerization with acrylic acid as the monomeric units and *N*,*N*′-methylenebisacrylamide as cross-linker (Supporting Information Figure S1). When immersed in acetone, the hydrogel film shrank and became opaque gradually due to the diffusion of the solvent into the gel, followed by the curving of the film, as well as an appearance of blister-like protuberances on the gel. Subsequently, the protuberances disappeared slowly, and a flat transparent flexible film was obtained (Figure 1a). When exposed to air, the acetone in the dehydrated gel evaporated, and flexible acetone-DPAA was retrieved. After the acetone-induced dehydration, the polymer network gradually collapsed and the inner structures of the gel transitioned from the porous hydrogel structure (Figure 1b, freeze-dried PAA hydrogel) to the lamella-like structures of acetone-DPAA (Figure 1c), which might have resulted from the phase separation in acetone, contrary to the behavior of the naturally air-dried PAA (air-DPAA), which appeared dense, and without microstructures (Figure 1d). Accordingly, the two gel types exhibited different mechanical properties. The acetone-DPAA was flexible and could be folded, twisted, and stretched, whereas the air-DPAA and freeze-dried PAA would break easily when subjected to bending (Supporting Information Figure S2).

To explain the change that occurred in the inner structure of the gels, we carried out a thermodynamic analysis of the hydrogel in the poor acetone solvent, according to the Flory–Huggins theory.[40,41] This system is a ternary mixture of three components, namely, a poor solvent (label 1), a suitable solvent (label 2), and polymer chains with different degrees of polymerization, N (label 3). Each component volume fraction is denoted by φ_i and the required incompressibility is expressed by:

$$\varphi_1+\varphi_2+\varphi_3=1 \tag{1}$$

The interactions between each pair of the components are of Flory–Huggins type, χ_{ij}. The equation of the free energy of the system is expressed by:

$$f=\varphi_1 ln\varphi_1+\varphi_2 ln\varphi_2+\frac{\varphi_3}{N} ln\varphi_3+\chi_{12}\varphi_1\varphi_2+\chi_{13}\varphi_1\varphi_3+\chi_{23}\varphi_2\varphi_3 \tag{2}$$

For a ternary system, the spinodal curve, defined as the limits of stability of the homogeneous phase, is given by:

DOI: 10.31635/ccschem.019.20190007

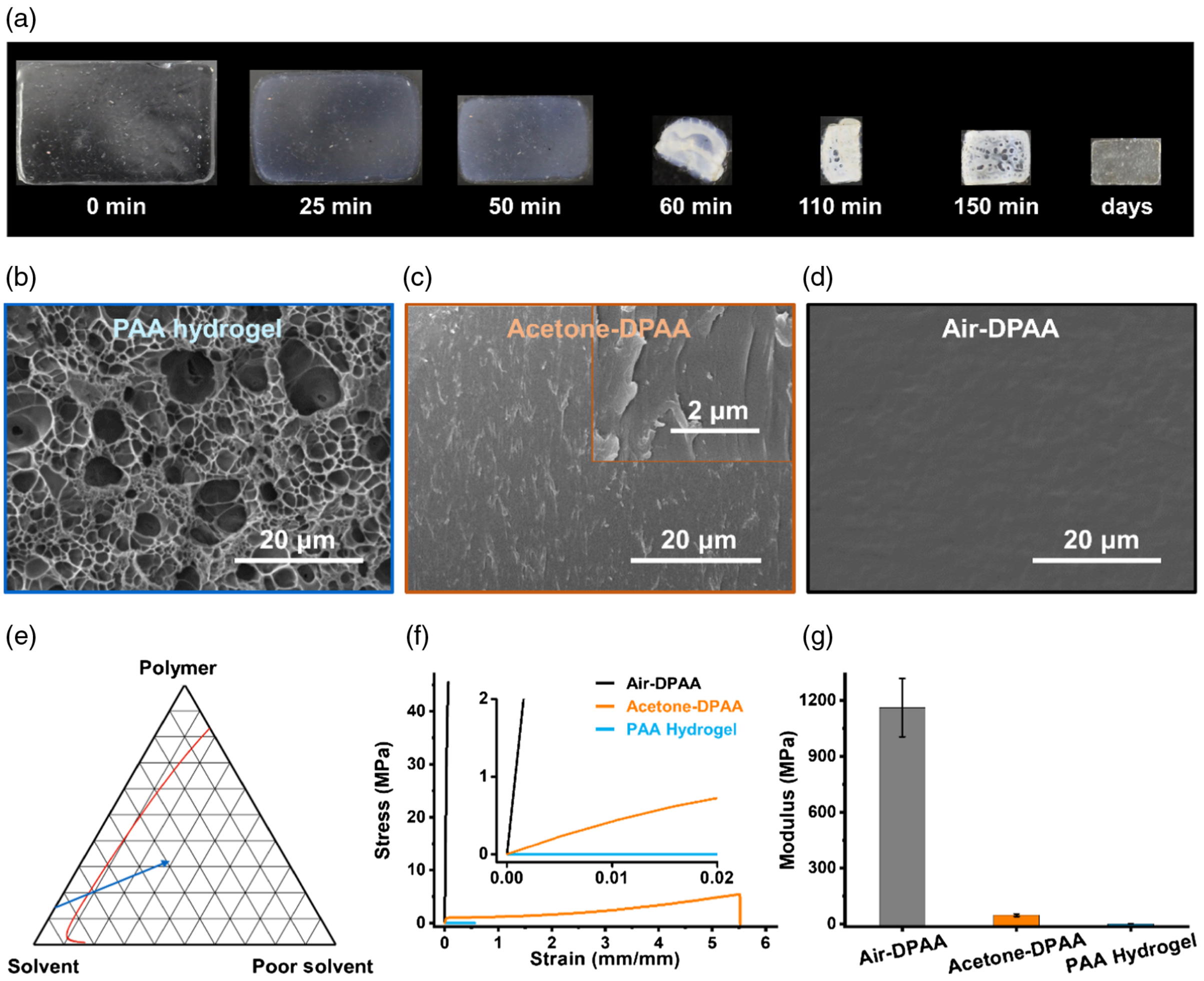

Figure 1 | *Dehydration of PAA hydrogel in acetone to generate flexible dry PAA gel. (a) The PAA hydrogel experienced a transparent–opaque–transparent process in acetone during which phase separation occurred. (b) The cross-sectional morphology of freeze-dried PAA hydrogel: porous structures. (c) The cross-sectional morphology of acetone-DPAA: lamella-like structures. (d) The cross-sectional morphology of air-DPAA: dense and without micro-structures. (e) The phase diagram of the ternary system: hydrogel, solvent, and nonsolvent. The red line is the binodal phase separation curves. The left side of it is homogenous phase and the right part is of two phases. The blue arrow indicates that increase of nonsolvent would lead to phase separation of the system. (f) Representative tensile stress–strain curves of air-DPAA, acetone-DPAA, and PAA hydrogel. Inset: tensile stress–strain curves at low strain. (g) Young's modulus,* E, *of the air-DPAA, acetone-DPAA, and PAA hydrogel.*

$$\begin{vmatrix} f_{11} & f_{12} \\ f_{21} & f_{22} \end{vmatrix} = 0 \qquad (3)$$

where

$$f_{11} = \frac{1}{\varphi_1} + \frac{1}{N\varphi_3} - 2\chi_{13}$$
$$f_{22} = \frac{2}{\varphi_2} + \frac{1}{N\varphi_3} - 2\chi_{23}$$
$$f_{12} = \frac{1}{N\varphi_3} + \chi_{12} - \chi_{13} - \chi_{23}.$$

Using the above expressions, we could calculate the spinodal curves (with $\chi_{12} = 0$, $\chi_{23} = 0$, and $\chi_{13} = 3$) as a simple case. Our typical experimental phase diagram is shown in Figure 1e, with its components consisting of the following: the poor solvent, the good solvent, and the polymer corresponding to acetone, water, and PAA hydrogel, respectively. The experimental system started from the left corner, where the bad solvent (acetone) concentration is zero. During the solvent-induced dehydration, in which there was a mutual diffusion of water and acetone, the acetone concentration in the gel increased gradually, indicated by the arrow in Figure 1e. When the system entered the instability region, it underwent phase separated into a polymer-rich and a polymer-poor part. However, as the polymer chains were cross-linked, it is unexpected that macrophase separation should take place, but it is plausible that microphase separation occurred, corresponding to the phase during which the gel displayed opaque appearance, which leads to the formation of layered structures.

Mechanical property of the acetone-DPAA film

To further explore the flexibility of the acetone-DPAA, a tensile machine was used to perform elongation tests on the hydrogel, solvent-dehydrated hydrogel, and air-dried gel at room temperature. Amazingly, the acetone-DPAA could be stretched to ~5.5 times its original length, without rupture (Figure 1d and Supporting Information Figure S3a). Figure 1f shows typical tensile stress–strain curves, which compares the acetone-DPAA with the air-DPAA, using the conventional PAA hydrogel as a control. The acetone-DPAA was capable of stretching, with an elongation at break of 5.5, and stress of 5.4 MPa at break. Meanwhile, the air-DPAA exhibited a rather low elongation of 0.066 at break and high stress of 45.5 MPa at break, which confirmed the flexibility of acetone-DPAA and the toughness and brittleness of the air-DPAA. Also, the elongation tests of the conventional PAA hydrogel control demonstrated fragile behavior, breaking easily before being stretched to strain = 1 (Figure 1f inset and Supporting Information Figure S3b). Young's modulus, E, calculated from the stress–strain curves (Figure 1g), revealed that the acetone-DPAA had an E of 46.8 MPa, similar to that of rubber, but much higher than that of the original PAA hydrogel with a negligible E (Figure 1g). However, the E of acetone-DPAA was much lower than that of the brittle air-DPAA (1160 MPa). Besides, the flexibility of the acetone-DPAA could be maintained even after air exposure for more than one month, reflecting its durability (Supporting Information Figure S4). These results verified that the lamella-like structures endowed the dried acetone-DPAA gels with flexibility and increased toughness, and stability, compared with the original PAA hydrogel and the air-DPAA gel.

Furthermore, the effects of the monomer and the cross-linker concentrations on the mechanical property of acetone-DPAA were investigated. Similar to the conventional hydrogel, the modulus of the acetone-DPAA increased gradually with the increase of cross-linker concentrations (Supporting Information Figure S5a,b). However, the monomer concentrations yielded a negligible effect on the mechanical property of acetone-DPAA. In addition, the representative tensile stress–strain curves of acetone-DPAA at varying AA concentrations revealed an almost overlapping effect (Supporting Information Figure S5c), which might be attributable to the complete collapse of the PAA hydrogel networks after treatment in acetone to generate acetone-DPAA, resulting in increased swelling ratio in a linear dimension, as the AA concentration increased (Supporting Information Figure S5d). Thus, on the whole, the increased monomeric concentration exhibited a slight influence on the acetone-DPAA network and their mechanical properties.

Mechanism of the flexibility of acetone-DPAA

Thermogravimetry (TG) was conducted to measure the actual water content of the air-DPAA, freeze-dried PAA, and acetone-DPAA to explore how their assumed water contents were affected by their corresponding structures, in particular, the flexibility of the dry PAA (Figure 2). According to the thermogravimetric and differential thermogravimetric (TG/DTG) curve of PAA hydrogel, the TG declined as the temperature increased to a stabilization point at 175 °C, which positively correlated with the loss of absorbed water (Supporting Information Figure S6).[42] At temperatures below 100 °C, the mass losses of air-DPAA, conventional freeze-dried PAA, and acetone-DPAA obtained were all small, 0.86%, 1.66%, and 2.26%, respectively. Alternatively, the mass losses increased to 4.82%, 7.01%, and 10.43%, respectively, at 175 °C, indicating the differences in absorbed water contents of the different gel types (Figure 2a). Also, the water content difference of the gel types might be attributable to the unique nanostructures adopted by the acetone-DPAA, which favored more vapor absorption. After that, we investigated the effect of the absorbed water on the flexibility of acetone-DPAA. Removal of the absorbed water in acetone-DPAA by subjecting to dryness after air exposure in the presence of anhydrous calcium chloride, ($CaCl_2$-acetone-DPAA), rendered the $CaCl_2$-acetone-DPAA stiff and brittle with an elongation at break of 0.09 (Figure 2b and Supporting Information Figure S7a), taking on a characteristic just like that of the air-DPAA. Upon subsequent air exposure at room temperature (~25 °C at relative humidity 36%) for 4 h, the $CaCl_2$-acetone-DPAA recovered its flexibility with an elongation at break of 4.8 times its original length (Figure 2b and Supporting Information Figure S7b). These results indicated that the inner lamella-like structure enhanced the absorbed water content of acetone-DPAA, and also, increased its flexibility, resulting in the transformation of the acetone-DPAA from a glassy state it should have acquired into a rubbery state.

In addition, the acetone-DPAA also exhibited humidity sensitivity, uncovered by measuring its tensile property at different humidities. As shown in Figure 2c and Supporting Information Figure S8, the acetone-DPAA demonstrated high sensitivity to moisture and exhibited a gradual decrease in modulus with increased air humidity; meanwhile, the elongation at break increased initially and then dropped. However, the air-DPAA did not show much sensitivity to humidity and was still easy to break with small elongation value (less than 0.1) at break, even when the humidity was as high as 70% (Supporting Information Figure S9). These results indicated that it was easier for the water vapor to diffuse into the acetone-DPAA than the air-DPAA.

Furthermore, differential scanning calorimetry (DSC) was applied to study the glass-transition temperature of

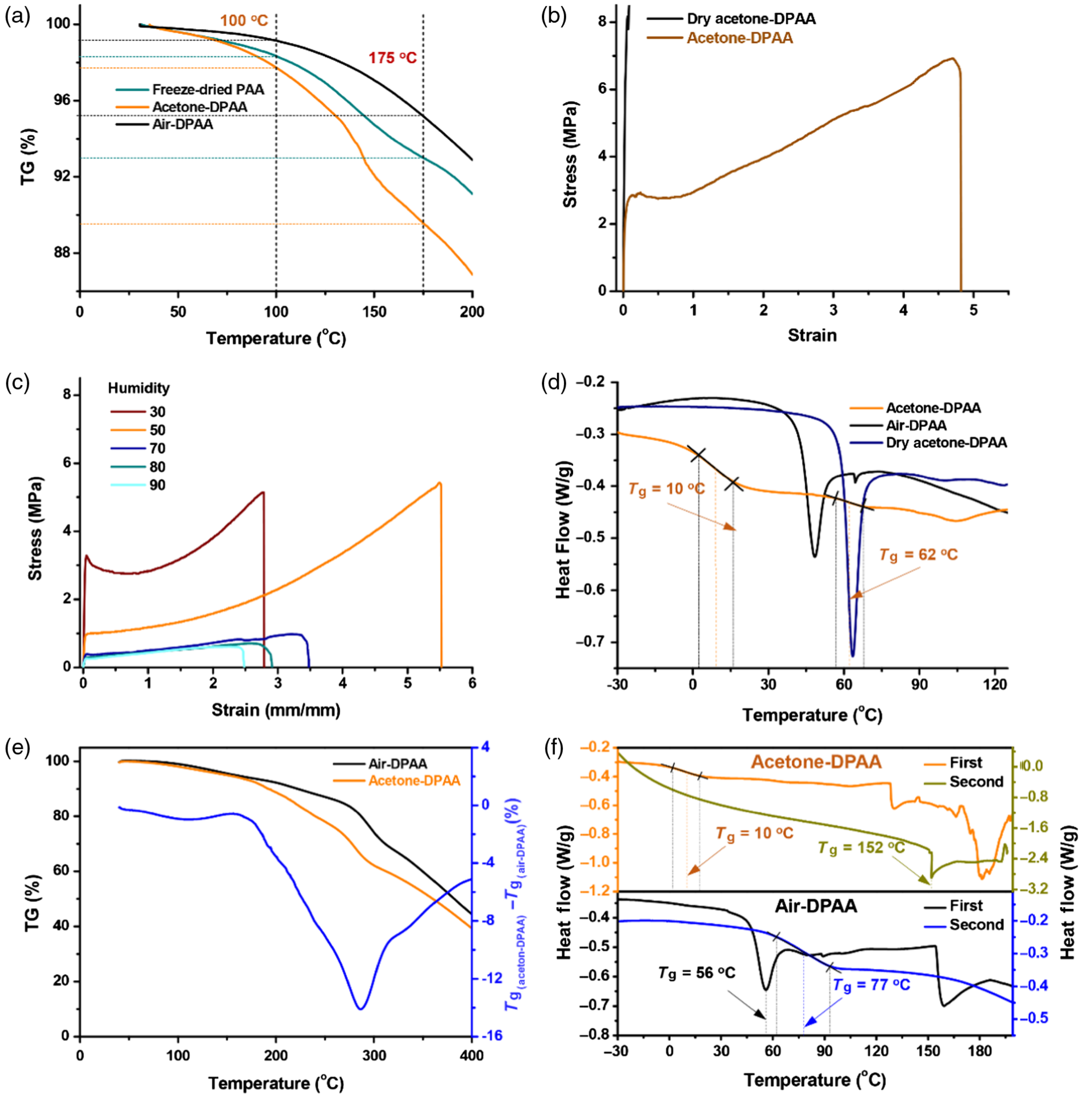

Figure 2 | *The effect of inner structure on the properties of dry PAA gels: acetone-DPAA, freeze-dried PAA, and air-DPAA. (a) The actual water content of the air-DPAA, freeze-dried PAA, and acetone-DPAA determined by TG. (b) Representative tensile stress–strain curves of $CaCl_2$-acetone-DPAA (dried with anhydrous $CaCl_2$) and restored acetone-DPAA in air (relative humidity of ~40% at 25 °C) for 4 h. (c) The acetone-DPAA exhibits humidity sensitivity. The representative tensile stress–strain curves of acetone-DPAA at different relative humidity at 25 °C. (d) DSC curves of air-DPAA, acetone-DPAA, and dry acetone-DPAA. The acetone-DPAA exhibits a T_g of 11.7 °C, which is less than room temperature. (e) The thermal degradation of acetone-DPAA and air-DPAA. According to the TG analysis, the acetone-DPAA is easier to decompose. (f) The DSC curves of acetone-DPAA (top) and air-DPAA (bottom) with two thermal cycles from −40 to 200 °C.*

air-DPAA, acetone-DPAA, and $CaCl_2$-acetone-DPAA (Figure 2d). In the DSC thermogram of acetone-DPAA, the glass-transition temperature (T_g) was observed at ~10 °C, much lower than room temperature at which acetone-DPAA acquired a rubbery state. In contrast, the air-DPAA, $CaCl_2$-acetone-DPAA, and freeze-dried PAA (Supporting Information Figure S10) remained in a glassy state at both temperatures. These results indicated that the lamella-like structures in acetone-DPAA made it easier for water adsorption, and the absorbed water, consequently, decreased its T_g value.[43-47] What is more, another T_g peak on the DSC curve of acetone-DPAA was visible at ~62 °C, which was similar to that of $CaCl_2$-acetone-DPAA, but different from the apparent T_g of air-DPAA at ~48 °C. Therefore, we presumed that incorporation of the inner lamella-like structure of the acetone-DPAA accounted for this difference, as well as the interaction of the polymer chains, which also, might have been altered during the solvent-induced dehydration.

To verify our speculation, the TG analysis of acetone-DPAA and air-DPAA were conducted (Figure 2e). Consistent with a previous report, indicating that, increase in temperature of PAA resulted in gradual decrease in the weight of the samples due to anhydride formation and carbon dioxide evolution,[48] our acetone-DPAA exhibited a higher decomposition rate at lower decomposition temperature than that of air-DPAA (Figure 2e). To further verify this difference between the two gel types, the DSC of acetone-DPAA and air-DPAA at two extreme thermal cycles (−30 to 200 °C) were conducted (Figure 2f). The DSC curves of acetone-DPAA during the first phase of temperature rise was similar to that in Figure 2d, whereby, the acetone-DPAA exhibited a much lower T_g than that of air-DPAA. Amazingly, after experiencing the first phase of temperature rise, there was a significant increase of the T_g of acetone-DPAA at ~150 °C, whereas the air-DPAA exhibited only a small increase of its T_g from 56 to 77 °C. These results indicated that the acetone-DPAA was much easier to decompose and be cross-linked than air-DPAA. This observation might be related to the distribution difference of interactions of inter- and intramolecular hydrogen bonding.[49-51] Further, we used Fourier transform infrared-attenuated total reflectance (FTIR-ATR) spectroscopy to explore the change of the air-DPAA and acetone-DPAA upon heat treatment at 155 °C for 20 h (Supporting Information Figure S11). The results also indicated that anhydride formation in acetone-DPAA was much easier than that in air-DPAA, a finding which, per a previous report, revealed that the anhydride formation occurred primarily by intramolecular reactions.[49] Thus, collectively, we deduced from our studies that when PAA hydrogel was immersed in acetone, phase separation occurred, accompanied by variations of inter- and intramolecular interactions, which resulted in the generation of the dense domain and the sparse domain with higher proportioned intramolecular (i.e., hydrogen bonds) interactions, whereby, the lamella-like structures were created, which both contributed to the flexibility of acetone-DPAA.

The generality of the solvent-induced dehydration for flexible dry gel

We verified the generality of the solvent-induced dehydration for flexible PAA dry gel by investigating if our approach would be applicable in some other hydrogels. Different poor solvents, including tetrahydrofuran (THF), acetonitrile (AN), and *N,N′*-dimethyformamide (DMF), miscible with water, were used to generate solvent-dehydrated PAA, poly(*N,N′*-dimethylacrylamide) (PDMA), and polyacrylamide (PAM) hydrogels. As shown in Figure 3 and Supporting Information Figure S12, in poor solvents, the hydrogels shrunk gradually, and became opaque, along with phase separation, which ultimately became transparent, except PAM in THF and DMF, which, although appeared opaque, remained brittle, similar to the results obtained by Gong and co-workers.[39] When air-dried further, the dry gels exhibited different flexibility (Figure 3, left insets): The THF-DPAA, AN-DPAA, and THF-DPDMA demonstrated flexibility characteristics similar to acetone-DPAA, and they could be twisted without any damage (Figure 3a–c, left insets), whereas the AN-DPDMA, THF-DPAM, and DMF-DPAM were brittle and easy to break when bent (Figure 3d–f, left insets). Observations made from micrographs of dry gel sections after scanning electron microscopy (SEM; Figure 3) revealed that the flexible dry gels exhibited lamella-like structures, whereas the brittle, dry gels displayed flat cross-sections or porous structures due to phase separation induced by the nonsolvent.[40,52,53] These lamella-like structures might have contributed to the

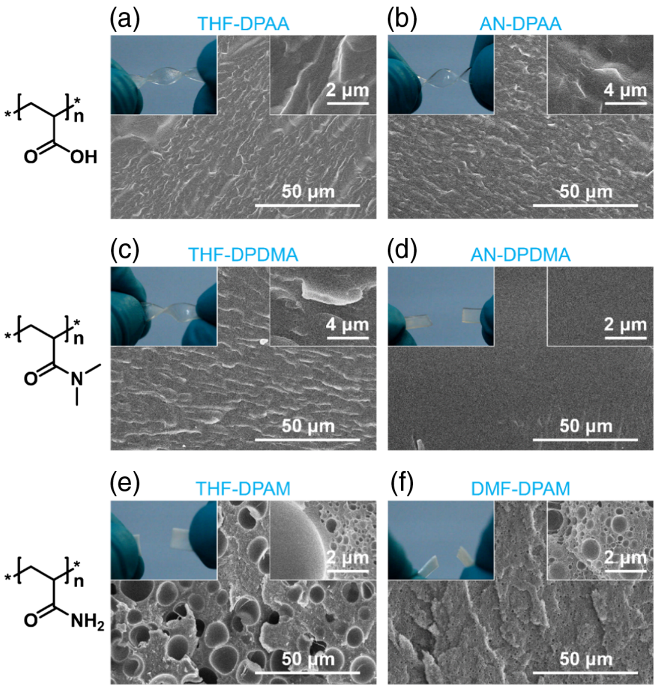

Figure 3 | *Flexibility and cross-sectional SEM images of dry gels from different hydrogels and their poor solvents. (a) THF-DPAA: flexible with lamella-like structure, (b) AN-DPAA: flexible with lamella-like structure, (c) THF-DPDMA: flexible with lamella-like structure, (d) AN-DPDMA: brittle without nanostructures, (e) THF-DPAM: brittle with porous structures, and (f) DMF-DPAA: brittle with porous structures. Insets: left, optical photographs of dry gels when twisted or bent, and right, higher magnification.*

transformation of the dry gels from brittle to ductile properties, which is consistent with our above inference. In essence, the inner structures and interactions of dry gel could be adjusted with solvent to realize their flexibility in air. However, extra efforts remain to be made from experiments and theories to elucidate the relationship between dry gel structure and solvents.

Self-healing performance of the acetone-DPAA films

This acetone-DPAA not only had excellent stretchability but also exhibited self-healing capability with the assistance of acetone (Figure 4a–c). As displayed in Figure 4a, the gel films were cut into halves; one set of halves were stained red with oil red and the other remained unstained. Then, the two sets of halves were brought together alternately. Afterward, the films were immersed in acetone at room temperature (25–30 °C) for 12 h before subjecting to mechanical test. The resultant healed acetone-DPAA films could be stretched, folded, and twisted without fracture (Figure 4b). Elongation tests were conducted on the healed acetone-DPAA films to quantify the self-healing efficiency (Supporting Information Figure S13). The healed gel could be

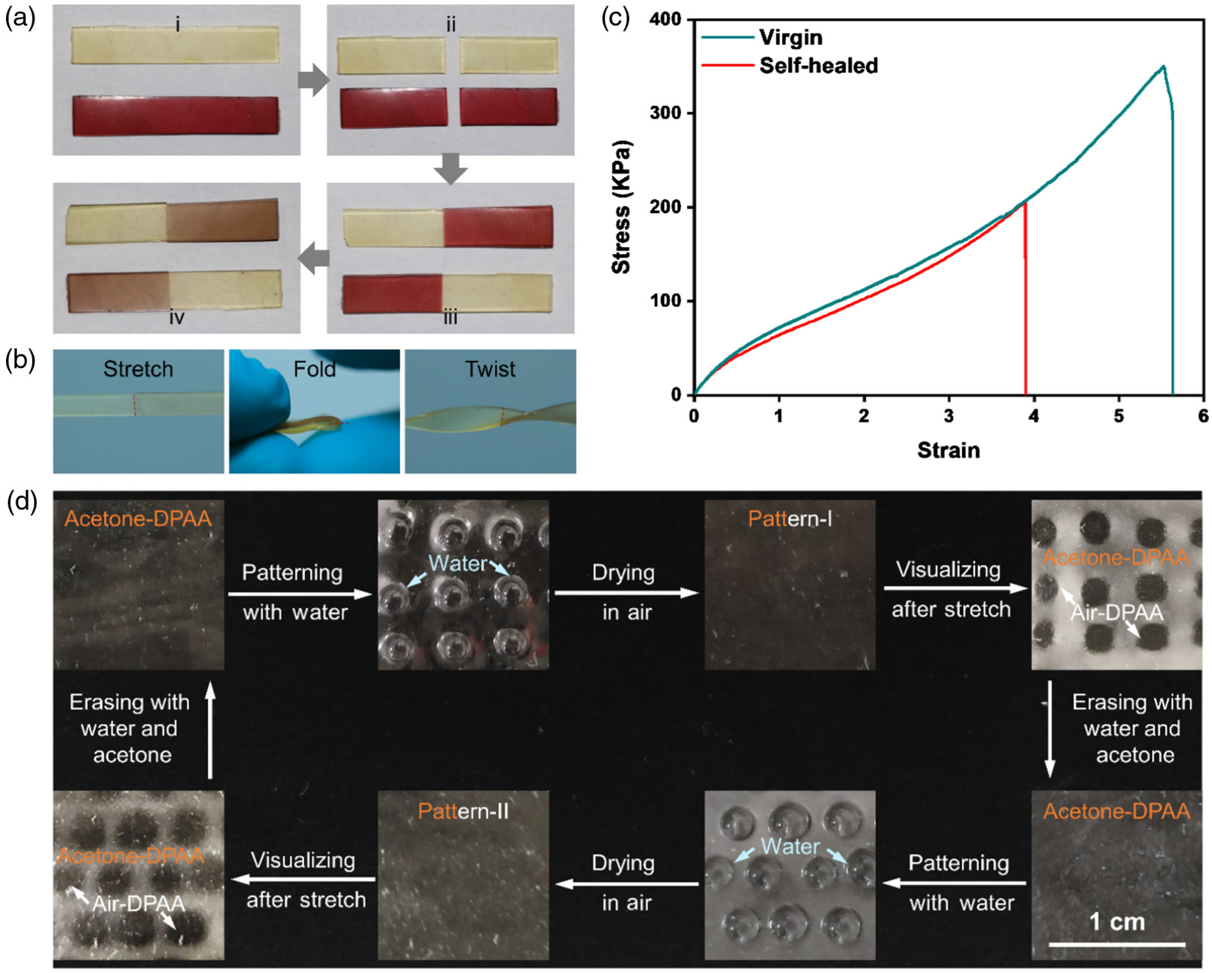

Figure 4 | *Self-healing capability and erasable stress-visualizing performance of the acetone-DPAA. (a) Photographs illustrating the self-healing process. Two pieces of acetone-DPAA film, one of which was stained as red with oil red (i), were cut into halves (ii). (iii) When two halves of the gel made contact, it enabled self-healing of the acetone-DPAA to occur. (iv) The self-healing was reinforced after immersed in acetone for 12 h. (b) The self-healed acetone-DPAA retained its flexibility, such that, it could be stretched, folded, and twisted without any damages. (c) Stress–strain curves of the virgin and self-healed acetone-DPAA. (d) An erasable stress-visualizing paper of acetone-DPAA film with water as ink. Water was dropped on the acetone-DPAA film in square arrangement and reswelled the local networks of PAA. When the water evaporated in air, the swollen networks collapsed again, and the air-DPAA was restored. Then invisible air-DPAA patterns were fabricated on the acetone-DPAA film. These patterns could be visualized after specific stretch. By immersing in water and acetone successively, the patterns were erased, and a renewed acetone-DPAA film was obtained. Using the same strategy, air-DPAA patterns in a triangular arrangement were fabricated and visualized.*

stretched ~4 times its original length, exhibiting a high healing efficiency of 65 ± 5%, calculated by obtaining the ratio between the elongations at break after healed relative to the elongations at break of the original acetone-DPAA film.[54–56] (Figure 4c). When the healed acetone-DPAA film was immersed in water, the film reswelled and was still easy to be separated at the interface by slight stretch (Supporting Information Figure S14), indicating that the interaction at the interface was destroyed by water. Therefore, we inferred that the self-healing capacity of flexible acetone-DPAA was attributed to its low modulus and the hydrogen bonding between –COOH and –COOH secondary interactions across the hydrogel structures.[55]

Writing/erasing performance of the acetone-DPAA films

In virtue of the difference in dehydration of PAA hydrogel in acetone and air, erasable low- to high-modulus patterns were fabricated. As illustrated in Figure 4d, the acetone-DPAA film worked as a flexible paper, and water was used as ink. Drops of water were applied on the gel film surface with the consequent reswelling of the local hydrogel networks of the film, adopting a square arrangement. Then the local-swollen hydrogel films were air-dried, air-DPAA patterns were acquired in acetone-DPAA film, which were invisible due to their similarity in optical properties (Supporting Information Figure S15). Interestingly, when the film was stretched (stress loading), the local air-DPAA patterns remained unchanged due to the attainment of high modulus. When the stress was unloaded, the acetone-DPAA gel parts became opaque due to the relaxation of the polymer chains, which then, rendered the patterns visible. Over a period (about 1 h at 40% humidity and 25–30 °C), the visible patterns vanished after restoration of the polymer chains (Supporting Information Figure S16). These patterns also erased with water and acetone successively, achieving a renewed acetone-DPAA film. In addition, different air-DPAA patterns in acetone-DPAA film in a triangular arrangement were fabricated, which could be visualized after stress was exerted, as before. Thus, this acetone-DPAA films were bestowed as a paper for erasable, strain-visualized information storage materials with water serving as ink, thereby, unveiling a novel carrier for confidential information.

Conclusions

We report a new approach that engineers the inner structures of dry hydrogels to optimize their flexibility via solvent-induced dehydration. The fabricated solvent-dehydrated gels exhibited high stretchability, self-healing capacity, and could maintain their flexibility in air. This flexibility might be attributable to the absorbed moisture and the lamella-like nanostructures acquired by the gels, leading to a decrease of their glass-transition temperature. The differences in the stretchability of the acetone-DPAA and air-DPAA enabled the flexible acetone-DPAA films to gain characteristics of strain-visualizing papers with writing/erasing performance, using water as invisible ink, and thus, promising for storage of confidential information. This solvent-induced dehydration-engineering strategy for flexible dry gels might initiate a new branch in the field of hydrogel chemistry and extend the scope of their potential applications.

Experimental Methods

Chemicals

Acrylic acid 99% (J&K Scientific, Beijing, China, Lot# LC80O82), acrylamide 99% (AAm; J&K, Lot# L510P42), *N,N′*-dimethylacrylamide 98% (DMA; J&K Scientific, Lot# LT60N21), *N,N′*-methylenebis(acrylamide) 98% (J&K Scientific, Lot#LT50N18), and ammonium persulfate 98% (J&K Scientific, Lot# LBBON03) were all used as received.

Preparation of hydrogel

The hydrogel films were prepared by free-radical polymerization in the spacer of two separated glass slides. The reaction solution was prepared by mixing monomer solution of 5 M AA, AAm, or DMA, with *N,N′*-methylenebis(acrylamide) as a cross-linker (mole ratio of divinyl to vinyl monomers, 2:400) and ammonium persulfate as initiator (10 mg in 1 mL reaction solution). The polymerization process proceeded in water bath set at 65 °C. After that, the prepared hydrogel was immersed in water for more than 3 days, and the water was exchanged at least three times during this period. First, a set of reaction solutions were prepared with varying AA concentrations of 2.5, 5, 7.5, and 10 M, and a fixed cross-linker of 1:200 to fabricate PAA hydrogel at different monomer concentrations. Second, another set of reaction solutions were prepared at a fixed AA concentration of 5 M and varying cross-linker ratios of 1:400, 2:400, 4:400, and 6:400.

Preparation of dry polymer gel

With PAA hydrogel as an example, the dry polymer gels obtained via solvent-induced dehydration were fabricated by immersing the hydrogel in organic solvents for more than 1 week, during which the solvents were replaced daily. The hydrogels experienced solvent exchange along with swelling or shrinking. Subsequently, the dry polymer gels were obtained after air evaporation of the residual solvents. The air-DPAA was fabricated via direct desiccation of the PAA hydrogel in air. The freeze-dried PAA was fabricated by freezing in liquid nitrogen and drying in freeze dryer. Whether the dry gels were flexible or brittle was assessed at 25 °C with a relative humidity of 35–40%.

TG analysis

The actual water content and thermostability of air-DPAA, freeze-dried PAA, and acetone-DPAA were measured with a Seiko Exstar 6300 TG/differential thermal analyzer. The TG was performed in nitrogen at a heating rate of 10 °C/min from 30 to 500 °C with the samples in aluminum pans.

Calculation of the swelling ratio in linear dimension of PAA gels

We described the vernier caliper measurements of swelling and shrinking performance of the gels using the following parameters: swelling ratio in linear dimension = d/d_0. d and d_0 are the widths of the gel films at equilibrium in acetone aqueous solution or air and water, respectively, defining the swelling ratio in a linear dimension of PAA gel in water as 1.

Elongation tests on the PAA gels

Elongation tests were conducted with temperature at 25 °C and relative humidity of ~40% (unless stated otherwise), using a commercial testing machine (Mark-10 ESM301L, Copiague, USA). The samples for elongation tests were fabricated from the PAA gel films by cutting into belts with widths of 5–8 mm. Then, the samples were clamped at both ends and elongated at a loading rate of 100 mm/min. The acetone-DPAA was kept at a specified humidity in an environmental chamber (KCL-2000W; EYELA, Tokyo, Japan) before used to investigate the effect of humidity on the mechanical property of acetone-DPAA.

Morphology of the gel films

The cross-sectional morphologies of the gels were characterized using a field-emission scanning electron microscopy (FESEM; JSM-7500F; JEOL, Japan) at 5 kV. The samples were prepared via freeze-drying in liquid nitrogen, and the cross-sections were obtained by breaking the polymer films in liquid nitrogen. All the samples were coated with thin layers of gold before FESEM observation.

Differential scanning calorimetry

For the DSC measurements, a Mettler-Toledo DSC 1 (Switzerland) was employed. A sample of 5–10 mg weight was placed in a sealed aluminum pan with a pore to connect the outside. The heating/cooling rates of 10 K/min were applied. Nitrogen was used as an inert gas, and an empty aluminum pan was used as reference, while liquid nitrogen was used as a cooling medium. Before the DSC measurements, the samples were kept in air at room temperature (25 °C) and relative humidity of 40–50%.

Supporting Information

Supporting Information is available.

Conflicts of Interest

The authors declare no competing financial interests.

Acknowledgments

This study is supported financially by the National Natural Science Foundation of China (21425314, 21501184, 21434009, 21421061, and 21504098), the Top-Notch Young Talents Program of China, Beijing Municipal Science & Technology Commission (Z161100000116037), and Youth Innovation Promotion Association, CAS (2017036). F.Z. designed and performed all the experiments. S.W. codesigned the experiments. Z.G., M.Y., S.L., Y.S., J.F., and J.M. conducted or supported the experiments for characterization. J.Z. conducted the thermodynamic analysis of the hydrogel in poor solvent. F.Z., L.J., P.W., and S.W. analyzed the data. F.Z. and S.W. wrote the article.

References

1. Seliktar, D. Designing Cell-Compatible Hydrogels for Biomedical Applications. *Science* **2012**, *336*, 1124–1128.
2. Chaudhuri, O.; Gu, L.; Klumpers, D.; Darnell, M.; Bencherif, S. A.; Weaver, J. C.; Huebsch, N.; Lee, H.-P.; Lippens, E.; Duda, G. N.; Mooney, D. J. Hydrogels with Tunable Stress Relaxation Regulate Stem Cell Fate and Activity. *Nat. Mater.* **2015**, *15*, 326–334.
3. Li, J.; Celiz, A. D.; Yang, J.; Yang, Q.; Wamala, I.; Whyte, W.; Seo, B. R.; Vasilyev, N. V.; Vlassak, J. J.; Suo, Z.; Mooney, D. J. Tough Adhesives for Diverse Wet Surfaces. *Science* **2017**, *357*, 378–381.
4. Peppas, N. A.; Hilt, J. Z.; Khademhosseini, A.; Langer, R. Hydrogels in Biology and Medicine: From Molecular Principles to Bionanotechnology. *Adv. Mater.* **2006**, *18*, 1345–1360.
5. Larson, C.; Peele, B.; Li, S.; Robinson, S.; Totaro, M.; Beccai, L.; Mazzolai, B.; Shepherd, R. Highly Stretchable Electroluminescent Skin for Optical Signaling and Tactile Sensing. *Science* **2016**, *351*, 1071–1074.
6. Kim, C.-C.; Lee, H.-H.; Oh, K. H.; Sun, J.-Y. Highly Stretchable, Transparent Ionic Touch Panel. *Science* **2016**, *353*, 682–687.
7. Calvert, P. Hydrogels for Soft Machines. *Adv. Mater.* **2009**, *21*, 743–756.
8. Zhang, F.; Fan, J.; Zhang, P.; Liu, M.; Meng, J.; Jiang, L.; Wang, S. A Monolithic Hydro/Organo Macro Copolymer Actuator Synthesized via Interfacial Copolymerization. *NPG Asia Mater.* **2017**, *9*, e380.

9. Zhang, X.; Wang, J.; Jin, H.; Wang, S.; Song, W. Bioinspired Supramolecular Lubricating Hydrogel Induced by Shear Force. *J. Am. Chem. Soc.* **2018**, *140*, 3186–3189.

10. Liu, M.; Ishida, Y.; Ebina, Y.; Sasaki, T.; Aida, T. Photolatently Modulable Hydrogels Using Unilamellar Titania Nanosheets as Photocatalytic Crosslinkers. *Nat. Commun.* **2013**, *4*, 2029.

11. Zhao, Z.; Zhang, K.; Liu, Y.; Zhou, J.; Liu, M. Highly Stretchable, Shape Memory Organohydrogels Using Phase-Transition Microinclusions. *Adv. Mater.* **2017**, *29*, 1701695.

12. Takushi, E.; Asato, L. I. U.; Nakada, T. Edible Eyeballs from Fish. *Nature* **1990**, *345*, 298–299.

13. Masuike, T.; Taki, S.; Hara, K.; Kai, S. Change of Temperature and Elastic Stiffness During Dehydration Process of Polyacrylamide Gel. *Jpn. J. Appl. Phys., Part 1* **1995**, *34*, 4997–5000.

14. Lakes, R. Materials with Structural Hierarchy. *Nature* **1993**, *361*, 511.

15. Peterlik, H.; Roschger, P.; Klaushofer, K.; Fratzl, P. From Brittle to Ductile Fracture of Bone. *Nat. Mater.* **2005**, *5*, 52–55.

16. Hahn, G. T. The Influence of Microstructure on Brittle Fracture Toughness. *Metall. Mater. Trans. A* **1984**, *15*, 947–959.

17. Schiller, K. Strength of Highly Porous Brittle Materials. *Nature* **1957**, *180*, 862.

18. Murphy, B. P.; Prendergast, P. J. The Relationship Between Stress, Porosity, and Nonlinear Damage Accumulation in Acrylic Bone Cement. *J. Biomed. Mater. Res.* **2002**, *59*, 646–654.

19. Phani, K. K.; Niyogi, S. K.; Maitra, A. K.; Roychaudhury, M. Strength and Elastic Modulus of a Porous Brittle Solid: An Acousto-Ultrasonic Study. *J. Mater. Sci.* **1986**, *21*, 4335–4341.

20. Currey, J. D. Mechanical Properties of Mother of Pearl in Tension. *Proc. R. Soc. Lond. B* **1977**, *196*, 443–463.

21. Aksay, I. A.; Trau, M.; Manne, S.; Honma, I.; Yao, N.; Zhou, L.; Fenter, P.; Eisenberger, P. M.; Gruner, S. M. Biomimetic Pathways for Assembling Inorganic Thin Films. *Science* **1996**, *273*, 892–898.

22. Giraud-Guille, M.-M. Plywood Structures in Nature. *Curr. Opin. Solid State Mater. Sci.* **1998**, *3*, 221–227.

23. Jackson, A. P.; Vincent, J. F. V.; Turner, R. M. The Mechanical Design of Nacre. *Proc. R. Soc. Lond. B* **1988**, *234*, 415–440.

24. Smith, B. L.; Schäffer, T. E.; Viani, M.; Thompson, J. B.; Frederick, N. A.; Kindt, J.; Belcher, A.; Stucky, G. D.; Morse, D. E.; Hansma, P. K. Molecular Mechanistic Origin of the Toughness of Natural Adhesives, Fibres and Composites. *Nature* **1999**, *399*, 761.

25. Ji, B.; Gao, H. Mechanical Properties of Nanostructure of Biological Materials. *J. Mech. Phys. Solids* **2004**, *52*, 1963–1990.

26. Barthelat, F.; Yin, Z.; Buehler, M. J. Structure and Mechanics of Interfaces in Biological Materials. *Nat. Rev. Mater.* **2016**, *1*, 16007.

27. Tang, Z.; Kotov, N. A.; Magonov, S.; Ozturk, B. Nanostructured Artificial Nacre. *Nat. Mater.* **2003**, *2*, 413–418.

28. Podsiadlo, P.; Kaushik, A. K.; Arruda, E. M.; Waas, A. M.; Shim, B. S.; Xu, J.; Nandivada, H.; Pumplin, B. G.; Lahann, J.; Ramamoorthy, A.; Kotov, N. A. Ultrastrong and Stiff Layered Polymer Nanocomposites. *Science* **2007**, *318*, 80–83.

29. Finnemore, A.; Cunha, P.; Shean, T.; Vignolini, S.; Guldin, S.; Oyen, M.; Steiner, U. Biomimetic Layer-by-Layer Assembly of Artificial Nacre. *Nat. Commun.* **2012**, *3*, 966.

30. Deville, S.; Saiz, E.; Nalla, R. K.; Tomsia, A. P. Freezing as a Path to Build Complex Composites. *Science* **2006**, *311*, 515–518.

31. Bai, H.; Walsh, F.; Gludovatz, B.; Delattre, B.; Huang, C.; Chen, Y.; Tomsia, A. P.; Ritchie, R. O. Bioinspired Hydroxyapatite/Poly(methyl methacrylate) Composite with a Nacre-Mimetic Architecture by a Bidirectional Freezing Method. *Adv. Mater.* **2016**, *28*, 50–56.

32. Mao, L. B.; Gao, H. L.; Yao, H. B.; Liu, L.; Colfen, H.; Liu, G.; Chen, S. M.; Li, S. K.; Yan, Y. X.; Liu, Y. Y.; Yu, S. H. Synthetic Nacre by Predesigned Matrix-Directed Mineralization. *Science* **2016**, *354*, 107–110.

33. Das, P.; Malho, J.-M.; Rahimi, K.; Schacher, F. H.; Wang, B.; Demco, D. E.; Walther, A. Nacre-Mimetics with Synthetic Nanoclays up to Ultrahigh Aspect Ratios. *Nat. Commun.* **2015**, *6*, 5967.

34. Erb, R. M.; Libanori, R.; Rothfuchs, N.; Studart, A. R. Composites Reinforced in Three Dimensions by Using Low Magnetic Fields. *Science* **2012**, *335*, 199–204.

35. Wang, J.; Lin, L.; Cheng, Q.; Jiang, L. A Strong Bio-Inspired Layered PNIPAM-Clay Nanocomposite Hydrogel. *Angew. Chem. Int. Ed.* **2012**, *51*, 4676–4680.

36. Suzuki, A.; Yamazaki, M.; Kobiki, Y. Direct Observation of Polymer Gel Surfaces by Atomic Force Microscopy. *J. Chem. Phys.* **1996**, *104*, 1751–1757.

37. Hirokawa, Y.; Jinnai, H.; Nishikawa, Y.; Okamoto, T.; Hashimoto, T. Direct Observation of Internal Structures in Poly(N-isopropylacrylamide) Chemical Gels. *Macromolecules* **1999**, *32*, 7093–7099.

38. Hirokawa, Y.; Okamoto, T.; Kimishima, K.; Jinnai, H.; Koizumi, S.; Aizawa, K.; Hashimoto, T. Sponge-Like Heterogeneous Gels: Hierarchical Structures in Poly(N-isopropylacrylamide) Chemical Gels as Observed by Combined Scattering and Confocal Microscopy Method. *Macromolecules* **2008**, *41*, 8210–8219.

39. Sato, K.; Nakajima, T.; Hisamatsu, T.; Nonoyama, T.; Kurokawa, T.; Gong, J. P. Phase-Separation-Induced Anomalous Stiffening, Toughening, and Self-Healing of Polyacrylamide Gels. *Adv. Mater.* **2015**, *27*, 6990–6998.

40. Altena, F. W.; Smolders, C. A. Calculation of Liquid–Liquid Phase Separation in a Ternary System of a Polymer in a Mixture of a Solvent and a Nonsolvent. *Macromolecules* **1982**, *15*, 1491–1497.

41. Huang, C.; de la Cruz, M. O.; Swift, B. W. Phase Separation of Ternary Mixtures: Symmetric Polymer Blends. *Macromolecules* **1995**, *28*, 7996–8005.

42. Tanaka, S.; Kaneti, Y. V.; Bhattacharjee, R.; Islam, M. N.; Nakahata, R.; Abdullah, N.; Yusa, S.-I.; Nguyen, N.-T.; Shiddiky, M. J. A.; Yamauchi, Y.; Hossain, M. S. A. Mesoporous Iron Oxide Synthesized Using Poly(styrene-b-acrylic acid-b-ethylene glycol) Block Copolymer Micelles as Templates for

Colorimetric and Electrochemical Detection of Glucose. *ACS Appl. Mater. Interfaces* **2018**, *10*, 1039–1049.

43. Nakamura, K.; Hatakeyama, T.; Hatakeyama, H. Differential Scanning Calorimetric Studies on the Glass Transition Temperature of Polyhydroxystyrene Derivatives Containing Sorbed Water. *Polymer* **1981**, *22*, 473–476.

44. Zeleznak, K. J.; Hoseney, R. C. The Glass Transition in Starch. *Cereal Chem.* **1987**, *64*, 121–124.

45. Oksanen, C. A.; Zografi, G. The Relationship Between the Glass Transition Temperature and Water Vapor Absorption by Poly(Vinylpyrrolidone). *Pharm. Res.* **1990**, *7*, 654–657.

46. Aguilera, J. M.; Levi, G.; Karel, M. Effect of Water Content on the Glass Transition and Caking of Fish Protein Hydrolyzates. *Biotechnol. Prog.* **1993**, *9*, 651–654.

47. Pouplin, M.; Redl, A.; Gontard, N. Glass Transition of Wheat Gluten Plasticized with Water, Glycerol, or Sorbitol. *J. Agric. Food. Chem.* **1999**, *47*, 538–543.

48. McGaugh, M. C.; Kottle, S. The Thermal Degradation of Poly(Acrylic Acid). *J. Polym. Sci., Part B: Polym. Lett.* **1967**, *5*, 817–820.

49. Eisenberg, A.; Yokoyama, T.; Sambalido, E. Dehydration Kinetics and Glass Transition of Poly(Acrylic Acid). *J. Polym. Sci., Part A: Polym. Chem.* **1969**, *7*, 1717–1728.

50. Otsu, T.; Quach, L. Head-to-Head Vinyl Polymers. III. Preparation and Characterization of Head-to-Head Poly(Acrylic Acid) and its Esters. *J. Polym. Sci., Polym. Chem. Ed.* **1981**, *19*, 2377–2389.

51. Maurer, J. J.; Eustace, D. J.; Ratcliffe, C. T. Thermal Characterization of Poly(Acrylic Acid). *Macromolecules* **1987**, *20*, 196–202.

52. Broens, L.; Altena, F. W.; Smolders, C. A.; Koenhen, D. M. Asymmetric Membrane Structures as a Result of Phase Separation Phenomena. *Desalination* **1980**, *32*, 33–45.

53. Smolders, C. A.; Reuvers, A. J.; Boom, R. M.; Wienk, I. M. Microstructures in Phase-Inversion Membranes. Part 1. Formation of Macrovoids. *J. Membrane Sci.* **1992**, *73*, 259–275.

54. Li, C. H.; Wang, C.; Keplinger, C.; Zuo, J. L.; Jin, L.; Sun, Y.; Zheng, P.; Cao, Y.; Lissel, F.; Linder, C.; You, X. Z.; Bao, Z. A Highly Stretchable Autonomous Self-Healing Elastomer. *Nat. Chem.* **2016**, *8*, 618–624.

55. Phadke, A.; Zhang, C.; Arman, B.; Hsu, C.-C.; Mashelkar, R. A.; Lele, A. K.; Tauber, M. J.; Arya, G.; Varghese, S. Rapid Self-Healing Hydrogels. *Proc. Natl. Acad. Sci. USA.* **2012**, *109*, 4383–4388.

56. Dai, X.; Zhang, Y.; Gao, L.; Bai, T.; Wang, W.; Cui, Y.; Liu, W. A Mechanically Strong, Highly Stable, Thermoplastic, and Self-Healable Supramolecular Polymer Hydrogel. *Adv. Mater.* **2015**, *27*, 3566–3571.

Supporting Information

Flexible Dry Hydrogel with Lamella-Like Structure Engineered via Dehydration in Poor Solvent

Feilong Zhang,[1,4] Jiajia Zhou,[2] Zhen Gu,[1] Man Yang,[1] Siheng Li,[1] Yongyang Song,[1] Jun-Bing Fan,[1] Jingxin Meng,[1] Peiyi Wu,[3] Lei Jiang[1,2,4] and Shutao Wang*,[1,4]

[1] CAS Key Laboratory of Bio-inspired Materials and Interfacial Science, CAS Center for Excellence in Nanoscience, Technical Institute of Physics and Chemistry, Chinese Academy of Sciences, Beijing 100190, P. R. China.

[2] Key Laboratory of Bio-Inspired Smart Interfacial Science and Technology of Ministry of Education, School of Chemistry, Beihang University, Beijing 100191, P. R. China.

[3] State Key Laboratory of Molecular Engineering of Polymers, Department of Macromolecular Science and Laboratory for Advanced Materials, Fudan University, Shanghai 200433, China.

[4] University of Chinese Academy of Sciences, Beijing 100049, P. R. China.

**Correspondence:* stwang@mail.ipc.ac.cn

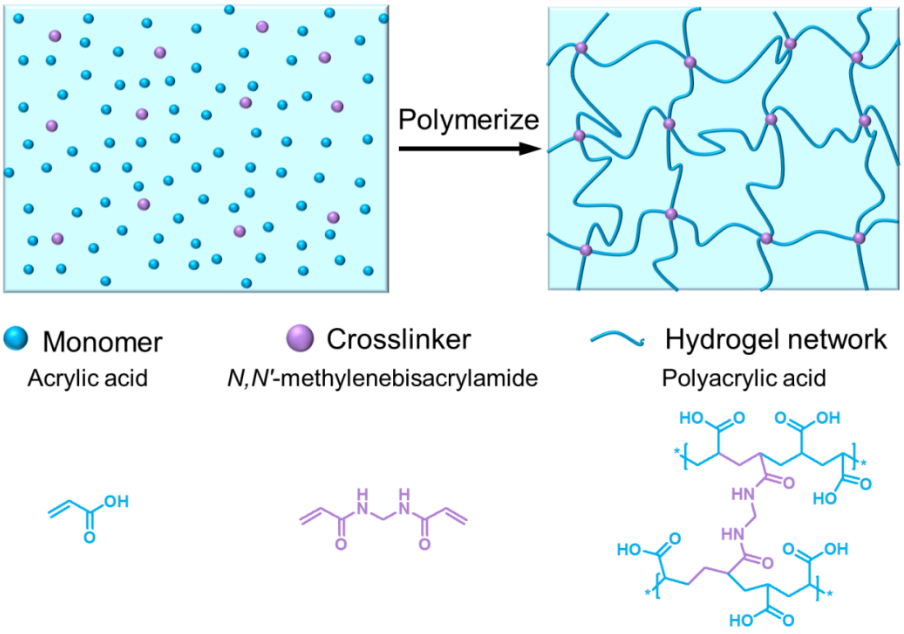

Figure S1. Preparation of PAA hydrogel. The original PAA hydrogel film was fabricated by free radical polymerization with acrylic acid as monomer, *N,N′*-methylenebisacrylamide as crosslinker and ammonium persulfate as initiator.

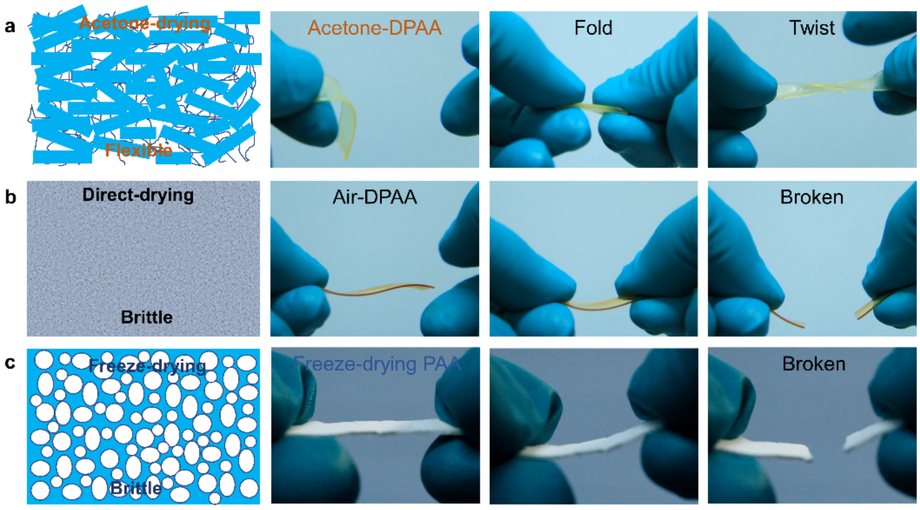

Figure S2. Flexibility of the acetone-DPAA, air-DPAA and freeze-dried PAA hydrogel.

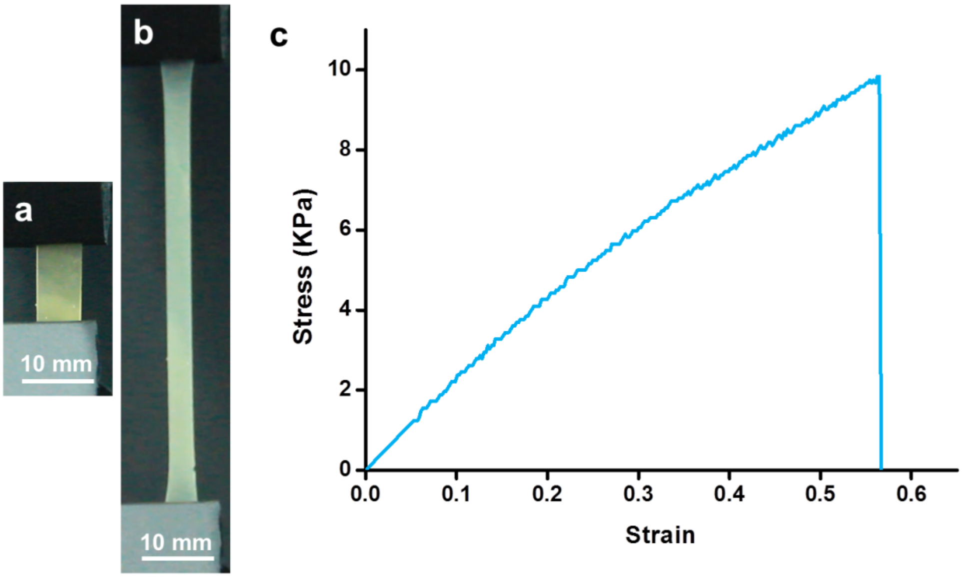

Figure S3. Tensile performance of acetone-DPAA and PAA gels. Photographs of the acetone-DPAA before (a) and after (b) stretching confirmed it flexibility. (c) Representative tensile stress-strain curves of PAA hydrogel.

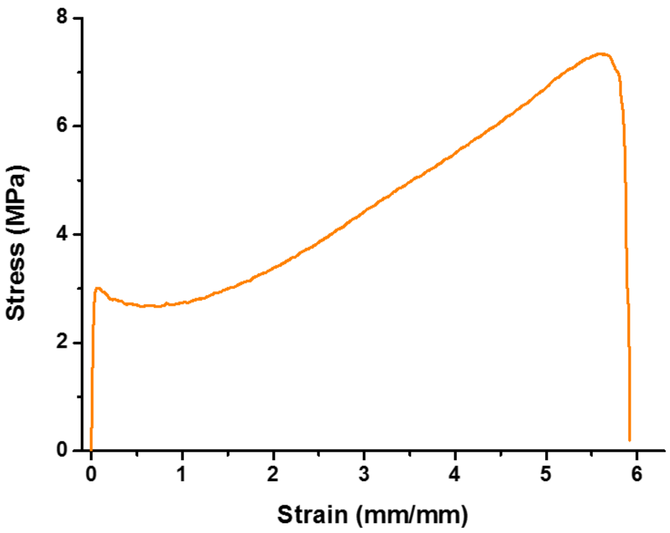

Figure S4. Tensile performance of the acetone-DPAA at humidity of 35% after exposed in air (humidity of 30%-40%) for more than one month.

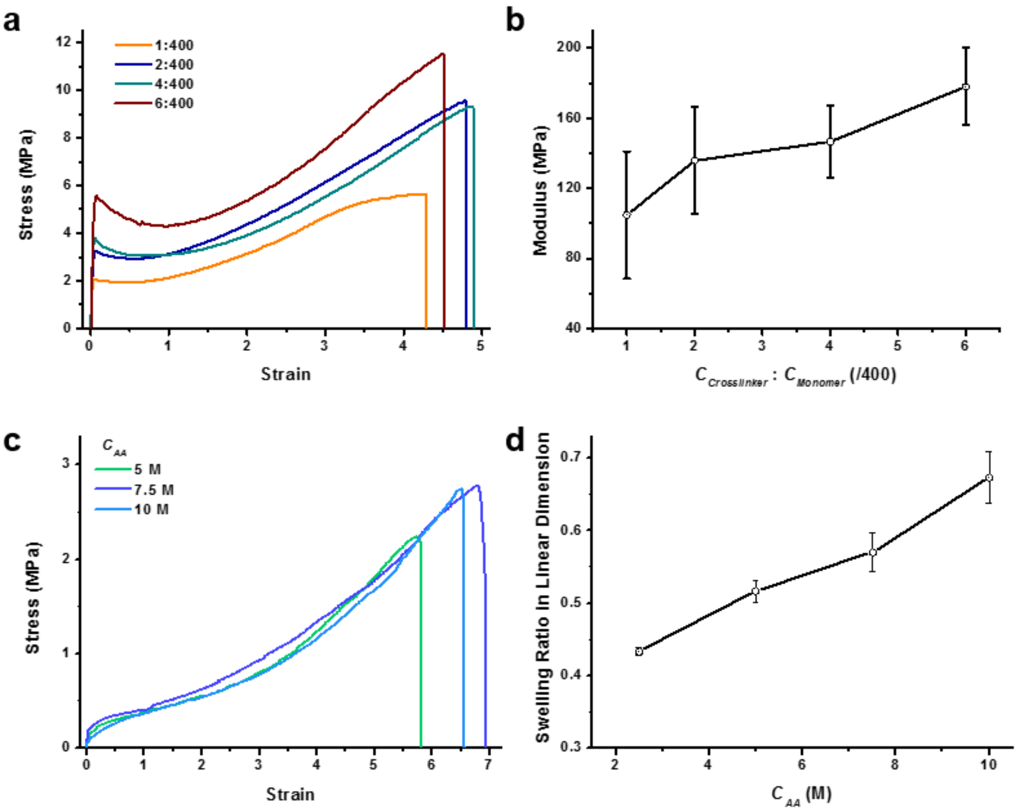

Figure S5. The effect of crosslinker and monomer concentrations on the mechanical properties of acetone-DPAA. (a) Stress-strain curves of acetone-PAA gels with different crosslinker concentrations. (b) The modulus of acetone-PAA gels increased with the increase of crosslinker concentrations. (c) Stress-strain curves of acetone-PAA gels with different monomer concentrations. (d) The swelling ratio in linear dimension of acetone-PAA gels with different monomer concentrations.

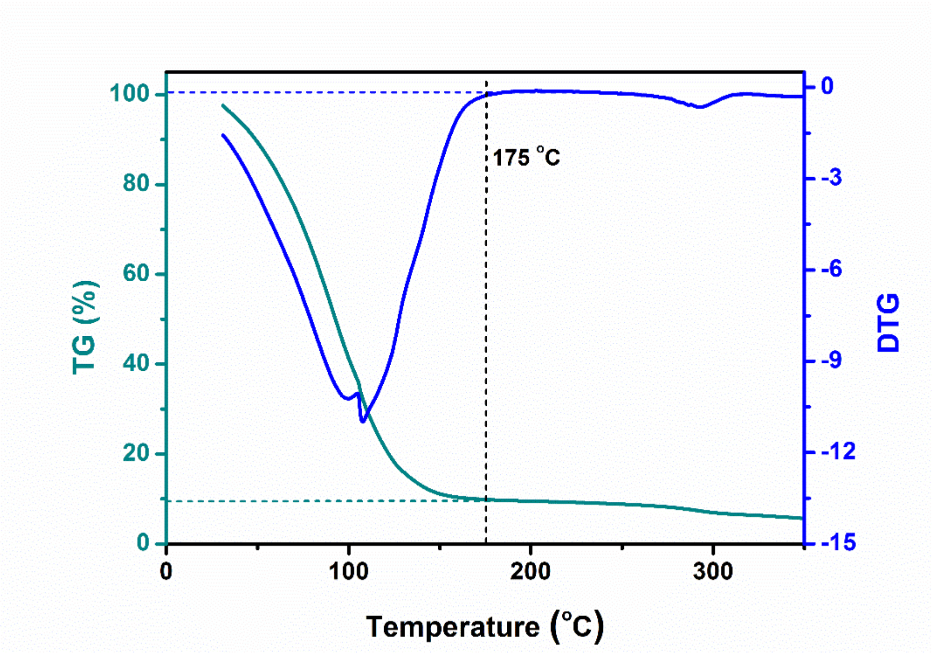

Figure S6. The free water and bound water in PAA hydrogel.

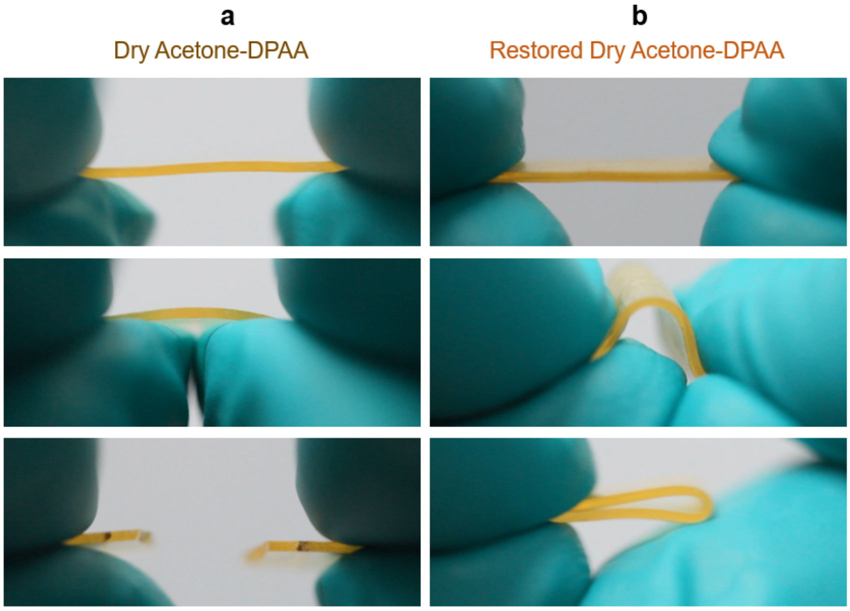

Figure S7. Images of the dry acetone-DPAA and restored dry acetone-DPAA when be bent. (a) The dry acetone-DPAA (dried with anhydrous calcium chloride) became stiff and brittle. When be bent, the dry acetone-DPAA broke into pieces. (b) Exposed into air (23.3 ^{o}C, relative humidity 36%), the dry acetone-DPAA restored its flexibility and can be buckled without damage.

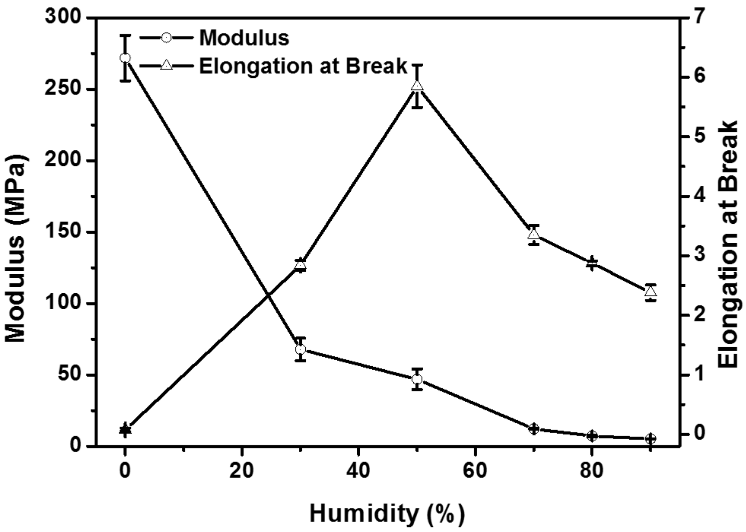

Figure S8. The modulus and elongation at break of acetone-DPAA at different relative humidity. At low humidity (dried with anhydrous $CaCl_2$), the acetone-DPAA is stiff and brittle. With the increase of humidity, the modulus of acetone-DPAA decreased, while the elongation at break increases first and then decreases with a maximum at humidity of 50%.

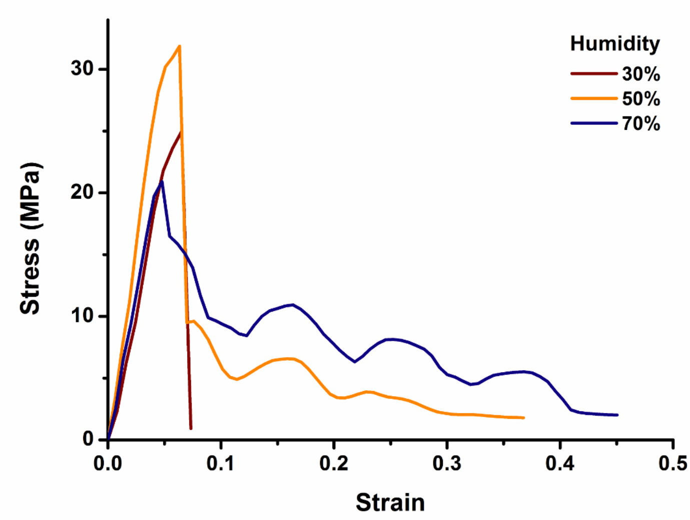

Figure S9. The representative tensile stress-strain curves of air-DPAA at different relative humidity, 25 °C. The air-DPAA is not such sensitive to humidity and still brittle compared with the acetone-DPAA.

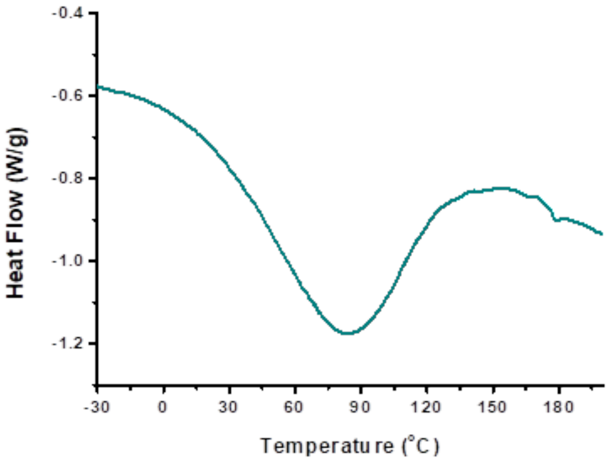

Figure S10. DSC curves of freeze-dried PAA (in air at 25 °C and relative humidity of ~40%). The glass transition temperature (T_g) was observed at about 80 °C.

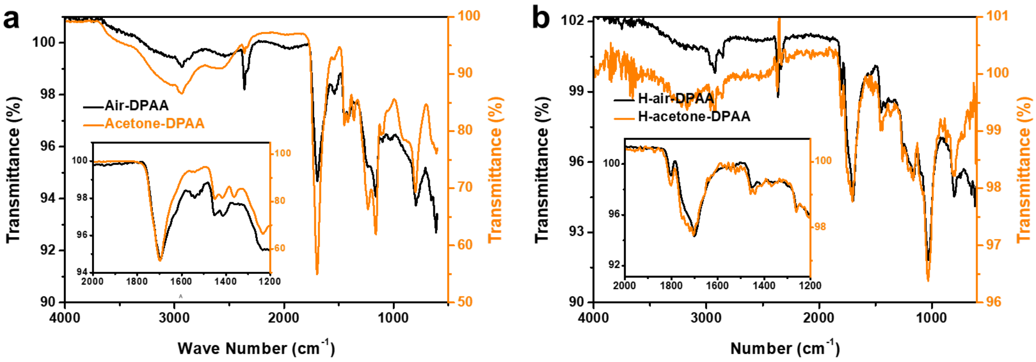

Figure S11. FTIR-ATR (attenuated total reflectance) Spectroscopy: a) as-prepared air-DPAA and acetone-DPAA; b) after heat-treatment at 155 °C for 20 h, named H-air-DPAA and H-acetone-DPAA.

FTIR-ATR (Excalibur 3100, Varian, USA)was used to explore the change of the air-DPAA and acetone-DPAA upon heat-treatment in nitrogen at 155 °C for 20 h. Compared with the as-prepared air-DPAA and acetone-DPAA (Figure S), the attenuation of the peak at 1700 cm^{-1} (carbonyl) and the appearance of new bands at 1750 cm^{-1}, 1800 cm^{-1} (assigned to carboxylic anhydride group) and 1020 cm^{-1}(assigned to C-O-C bending vibration of the acid anhydride) in the infrared spectra of H-air-DPAA and H-acetone-DPAA indicated the anhydride formation. The peak area ratio of bands at 1750 cm^{-1} and 1800 cm^{-1} to that at 1700 cm^{-1} in H-acetone-DPAA is much higher the that in H-air-DPAA, which indicated that anhydride formation in acetone-DPAA is much easier to than that in air-DPAA. To some extent, these results verified the ratio of intramolecular hydrogen bonds to intermolecular hydrogen bonds is higher in acetone-DPAA than in air-DPAA.

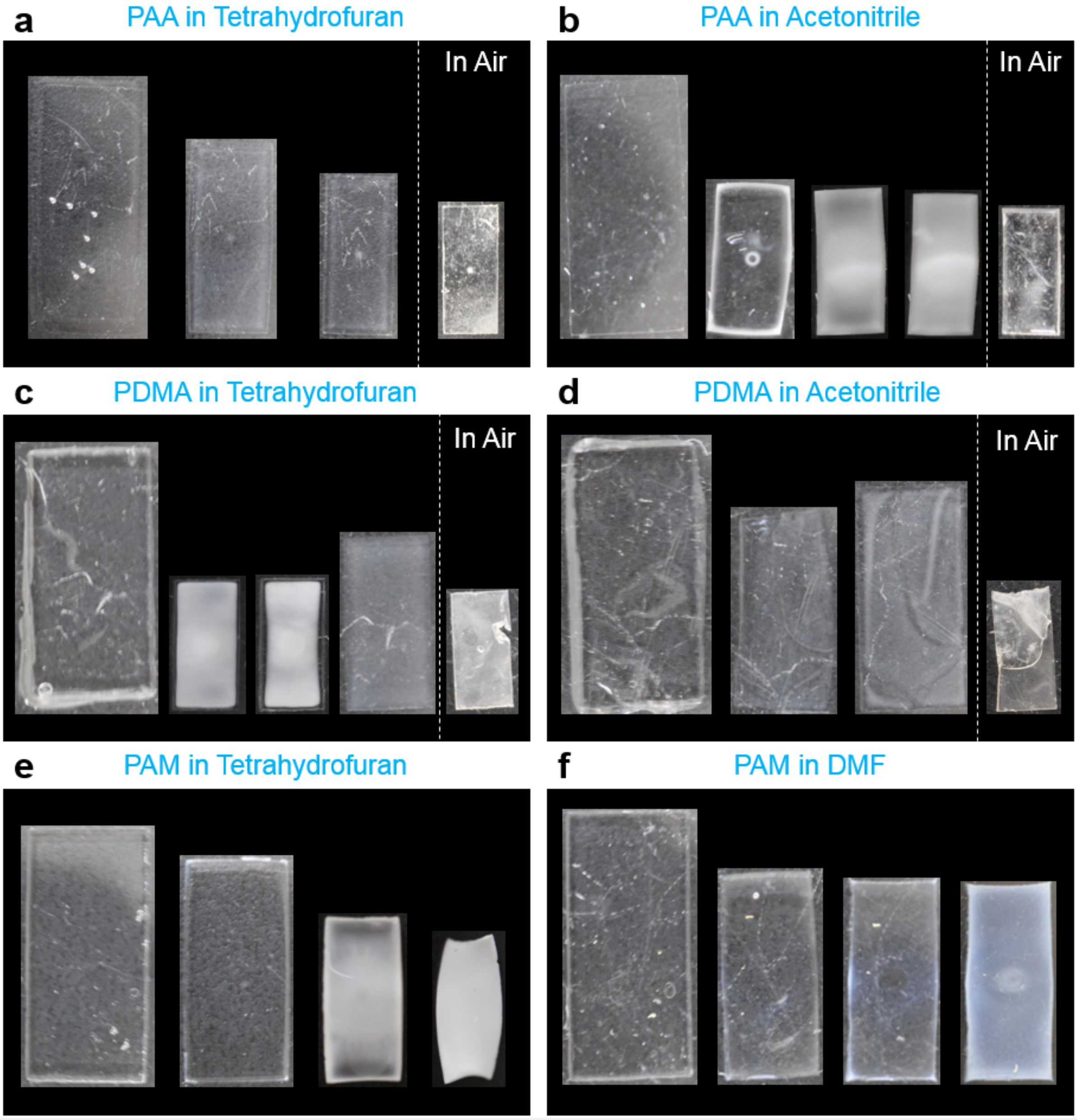

Figure S12. Hydrogels in their poor solvents. (a) PAA hydrogel in THF; (b) PAA hydrogel in AN; (c) PDMA hydrogel in THF; (d) PDMA hydrogel in AN; (e) PAM hydrogel in THF; (f) PAM hydrogel in DMF.

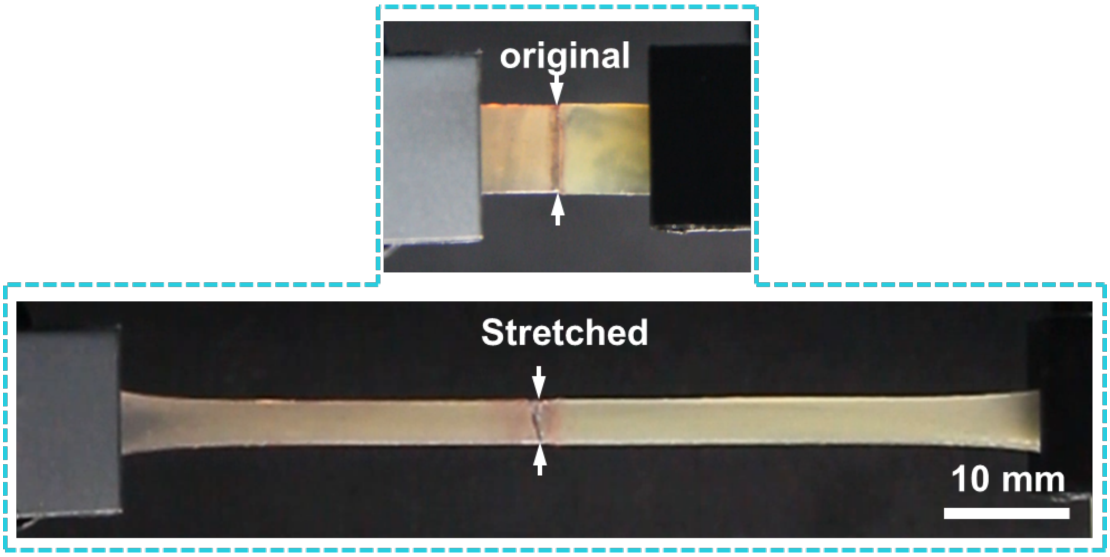

Figure S13. Self-healing performance of the acetone-DPAA. Photographs demonstrated the stretchability of the self-healed acetone-DPAA, which can reached almost four times its original length.

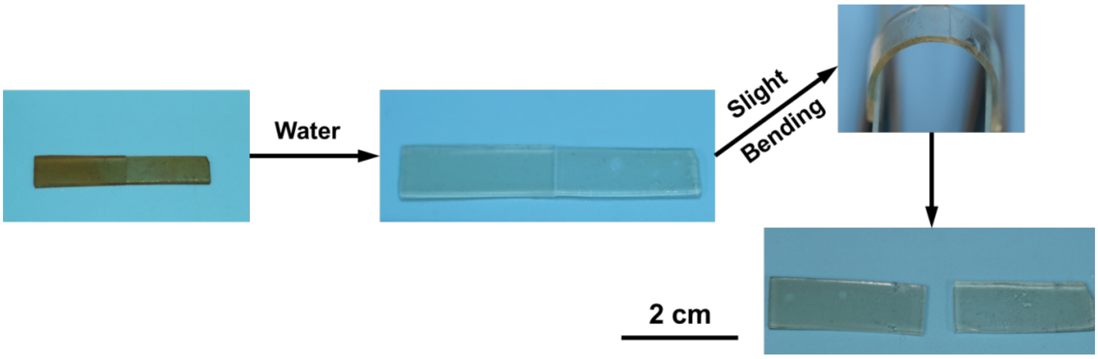

Figure S14. The healed acetone-DPAA gel was immersed in water. The gel swelled gradually, which could tolerate slight bending, but is still easy to separate at the interface by slight stretch.

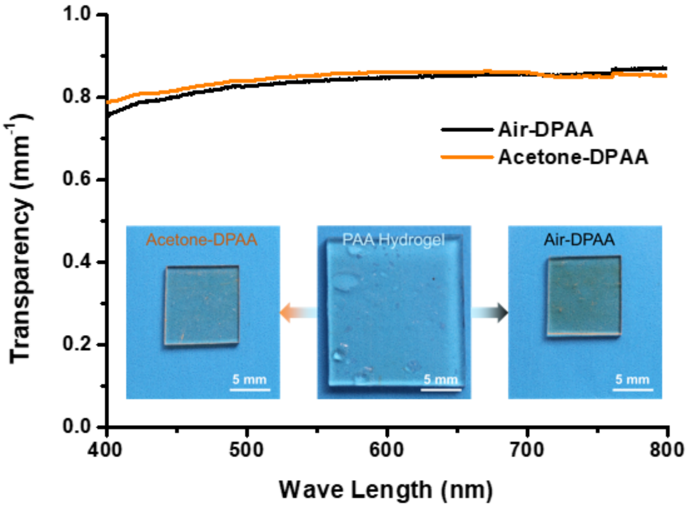

Figure S15. The transparency of air-DPAA and acetone-DPAA. The acetone-DPAA and air-DPAA exhibited similar transmissivity from 400 nm to 800 nm (using a UV-Vis Spectrophotometer, UV-2550, SHIMADZU, Japan).

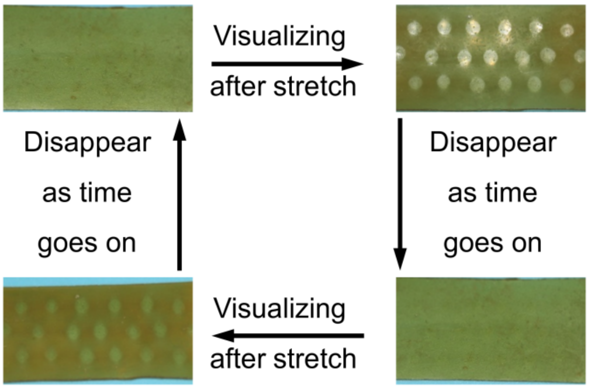

Figure S16. The time dependence of visualized air-DPAA/acetone-DPAA patterns. The air-DPAA patterns on acetone-DPAA film were visualized after a stretch as the acetone-DPAA part became opaque. The patterns disappeared when the visualized patterns was placed in air for a while. These patterns could be re-visualized after a second stretch, which disappeared again after a certain time of standing in air.